Research Article
doi.org/10.1002/elsa.202300025

Chemistry Europe
European Chemical Societies Publishing

Received: 19 September 2023
Revised: 14 December 2023
Accepted: 19 December 2023

Sustainable supercapacitor with a natural rubber-based electrolyte and natural graphite-based electrodes

Kumudu S. Perera[1] | **Kamal P. Vidanapathirana**[1] | **Lewis J. Adams**[2] | **Nilanthy Balakrishnan**[2]

[1]Department of Electronics, Faculty of Applied Sciences, Wayamba University of Sri Lanka, Kuliyapitiya, Sri Lanka

[2]School of Chemical and Physical Sciences, Keele University, Keele, UK

Correspondence
Kumudu S. Perera, Department of Electronics, Faculty of Applied Sciences, Wayamba University of Sri Lanka, Kuliyapitiya, Sri Lanka.
Email: kumudu@wyb.ac.lk

Nilanthy Balakrishnan, School of Chemical and Physical Sciences, Keele University, Keele, ST5 5BG, UK.
Email: n.balakrishnan@keele.ac.uk

Funding information
Engineering and Physical Sciences Research Council, Grant/Award Number: EP/Y003462/1; Keele University; Wayamba University of Sri Lanka

Abstract

Supercapacitors are at the forefront of energy storage devices due to their ability to fulfill quick power requirements. However, safety and cost are important parameters for their real-world applications. Green materials-based electrodes and electrolytes can make them safer and cost-effective. Herein, a supercapacitor based on a methyl-grafted natural rubber/salt-based electrolyte and natural graphite (NG)-based electrodes are fabricated and characterized. Zinc trifluoromethanesulfonate [$Zn(CF_3SO_3)_2$] is used as the salt for the electrolyte. A mixture of NG, activated charcoal, and polyvinylidenefluoride is used for electrodes. Our supercapacitor shows a single electrode specific capacitance, C_{sc} of 4.2 Fg^{-1} from impedance measurement. Moreover, the capacitive and resistive features are dominant at low and high frequencies, respectively. The cyclic voltammetry test shows the dependence of C_{sc} on the scan rate with a high value at slow scan rates. Performance of the supercapacitor during 5000 charge and discharge cycles at a constant current of 90 μA shows a rapid decrease of single electrode specific discharge capacitance at the beginning, but it starts to stabilize after about 2500 cycles. These findings are relevant to further developments of green materials-based supercapacitors, offering opportunities to expand the functionalities of supercapacitors in green technologies.

KEYWORDS
natural graphite, natural rubber, supercapacitors, zinc trifluoromethanesulfonate

1 | INTRODUCTION

Attention on supercapacitors is being driven forward at an enormous speed due to their extraordinary power capability than conventional capacitors. On the other hand, they have been identified as the connectors bridging the gap between conventional capacitors and batteries in terms of power and energy.[1] The structure of a supercapacitor is similar to a common electrochemical device with two electrodes and an electrolyte which serves as the passage for ions to travel between the electrodes. At present, supercapacitors have been successfully used for a diverse range of applications such as automobiles, communication, entertainment, and medical purposes. Due to the high demand, a surge of investigations is being carried out on supercapacitors to further improve their features including safety

Research Article
doi.org/10.1002/elsa.202300025
Chemistry Europe
European Chemical Societies Publishing

and cost. In par with novel concepts in green technology around the globe, attempts have been geared to exploit natural materials to be used as electrolytes and electrodes of supercapacitors. One such methodology is developing polymer electrolytes using natural polymers to replace the liquid electrolytes which have been commonly used for many of the available supercapacitors in the market.[2,3] At the beginning of the 21st century, a massive interest was paid on natural rubber (NR) to be used in polymer electrolytes instead of commercially available toxic polymers. Before that, NR has been considered only for manufacturing different items varying from toys to automobiles. Due to the insulating nature of NR, it is required to modify its structure enabling it to serve as a polymer to be used for electrolytes. There are two main modification methods, such as grafting and epoxidization.[4] Under grafting, a certain number of methyl groups are grafted to the NR backbone. A methyl-grafted NR is labeled with the number of methyl groups grafted like MG49-NR and MG30-NR. MG49-NR has received more attention as it has the highest number of methyl groups (49%) grafted to the NR backbone. In the process of epoxidation, hydrophilic groups are introduced along the NR backbone, and the structure is modified chemically. However, many researchers have used the grafting method due to some drawbacks with epoxidized NR. With the continuous research activities and their progress, researchers have employed NR-based polymer electrolytes in different applications including batteries and supercapacitors.[5]

Another approach that has been identified to improve safety and cut down the price of supercapacitors is using natural materials for electrodes. In that line, natural graphite (NG) is a promising material due to its presence as a natural resource in many countries. Currently, it has been employed as a battery electrode material with the limelight of its prominent electronic conductivity.[6,7] As far as its candidacy for supercapacitor electrodes is concerned, there is a drawback due to its inherent low surface area. For high performance in supercapacitors, the high surface area is one of prime importance to accommodate more charge storage. However, many research groups working on graphite and supercapacitors have attempted several approaches to overcome this challenge.[6,7] One of the trials is ball milling NG whereby it is expected to exfoliate graphite using lateral force which allows an increase in the surface area.[8,9] The end product is a few nanolayers of graphene of which the structure is two-dimension and hence has a larger surface area. Reduced graphene oxide (rGO) also has a large surface area. Pandey et al. have prepared rGO using NG and they have successfully fabricated a supercapacitor using rGO electrodes.[10] They have reported a specific capacitance value of about 17 Fg^{-1}. As another attempt, some have prepared composite electrodes by incorporating high surface area materials such as activated carbon with NG for supercapacitor electrodes.[11] A significant performance improvement has been observed with such composite electrodes.

In this study, we fabricated and characterized a supercapacitor based on 49% poly(methyl methacrylate) (PMMA) grafted NR (MG49-NR) and $Zn(CF_3SO_3)_2$ salt-based solid-polymer electrolyte and NG composite electrodes. The electrolyte was characterized using X-ray diffraction (XRD) and attenuated total reflection Fourier-transform infrared spectroscopy (ATR-FTIR), which confirms that the $Zn(CF_3SO_3)_2$ salt is solvated well in the MG49-NR polymer matrix. The supercapacitor was characterized using electrochemical impedance spectroscopy (EIS), cyclic voltammetry (CV) test, and galvanostatic charge-discharge (GCD) test. According to our knowledge, this is the first investigation for a supercapacitor with the MG49-NR + Zn salt-based electrolyte and NG composite electrodes.

2 | RESULTS AND DISCUSSION

The electrolyte was prepared using 49% PMMA grafted NR (MG49-NR) and $Zn(CF_3SO3)_2$ by solvent casting method (see Supplementary Information S1 for detailed preparation method). The prepared electrolyte shows a conductivity of 0.6×10^{-4} Scm^{-1} at room temperature. Figure 1a,b shows the structure of MG49-NR and $Zn(CF_3SO_3)_2$.[12,13] Surface-sensitive ATR-FTIR was used to study the vibrational energies of covalent bonds in MG49-NR and the chemical interactions that occur in the complex of MG49-NR + $Zn(CF_3SO_3)_2$, see Figure 1c. The major regions of interest are the oxygen atoms of the carbonyl group (—C = O) (1740 – 1700 cm^{-1}) and the ether group (C—O—C) (1250–1050 cm^{-1}) from the PMMA structure in the MG49-NR. The symmetrical stretching of the carbonyl group ν(—C = O) at the wavenumber of 1727 cm^{-1} in PMMA is slightly broadened and shifted to 1725 cm^{-1} being after blended with $Zn(CF_3SO_3)_2$ salt. This confirms that the C = O carbonyl group experiences a weak stretching mode due to strong intermolecular interaction. In other words, the bonding length of ν(—C = O) of PMMA becomes longer because the high electronegative value of oxygen atoms pulls the Zn^{2+} ions toward the central atoms, thus stretching the bond between the carbon and oxygen in the carbonyl group. This intermolecular attraction also affected the vibrational band for the —O—CH_3 group. This band shifted to a higher wavenumber from 1447 to 1449 cm^{-1} after the incorporation of the $Zn(CF_3SO_3)_2$ salt into the MG49-NR polymer matrix. This blueshift indicates a stronger asymmetry stretch between the oxygen and the methyl group. These shifts in the vibrational bands

Research Article
doi.org/10.1002/elsa.202300025
Chemistry Europe
European Chemical Societies Publishing

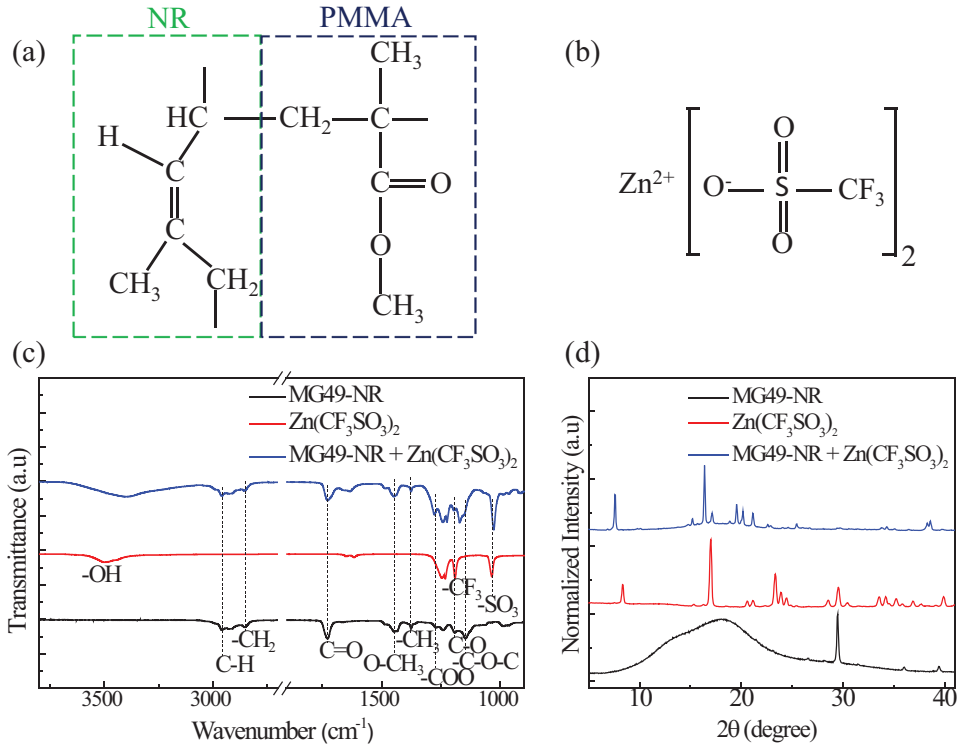

FIGURE 1 Schematic structure of (a) MG49-NR polymer and (b) $Zn(CF_3SO_3)_2$ salt. (c) Attenuated total reflection Fourier-transform infrared spectroscopy (ATR-FTIR), and (d) X-ray diffraction (XRD) spectra of MG49-NR polymer, $Zn(CF_3SO_3)_2$ salt, and MG49-NR + $Zn(CF_3SO_3)_2$ polymer-salt complex.

confirm the formation of the polymer-salt complex. Moreover, the peaks corresponding to the asymmetrical stretching of ν_{as}(—C—O—C) at 1147 cm^{-1} and symmetrical stretching of ν_s(—COO—) at 1271 cm^{-1} in MG49-NR shifted to 1154 and 1278 cm^{-1}, respectively after the incorporation of $Zn(CF_3SO_3)_2$ salt. This strong stretching is due to the changes in electronegativity of the double bond's carbon with oxygen which coordinated with Zn^{2+}. These results indicate a strong intermolecular interaction between oxygen from the carbonyl group of PMMA in MG49-NR with Zn-ions. Similar observations were reported by Whba et al. when incorporating Li-based salts with MG49-NR.[12] They mentioned that the oxygen atoms on the MG49-NR polymer chain act as an electron donor and form a coordinate/dative bond with the lithium ions from the doping salts to form a polymer-salt complex. This could be the same for the incorporation of Zn-based salt with MG49-NR. Moreover, the symmetric stretching vibrational mode of ν_s(—SO_3) at 1035 cm^{-1} and asymmetric stretching of ν_{as}(—CF_3) at 1190 cm^{-1} in $Zn(CF_3SO_3)_2$ salt shifted to lower wavenumbers of 1028 and 1171 cm^{-1}, respectively after being blended with MG49-NR polymer. This weak stretching confirms that the bonding lengths of ν_s(—SO_3) and ν_{as}(—CF_3) become longer due to the changes in the high electronegative value of oxygen atoms pulled the Zn^{2+} ions toward the —C = O of PMMA in MG49-NR. Complete tables of ATR-FTIR peak positions of MG49-NR polymer, $Zn(CF_3SO_3)_2$ salt, and MG49-NR + $Zn(CF_3SO_3)_2$ polymer matrix are given in Supporting Information S2.

XRD is used to analyze the crystallinity nature of MG49-NR, $Zn(CF_3SO_3)_2$ salt and MG49-NR + $Zn(CF_3SO_3)_2$ polymer-salt complex, see Figure 1d. The XRD pattern of MG49-NR shows a hump in the region between 10° and 23° and well-defined narrow peaks at 2θ = 29.5°, 36.0°, and 39.5° which is attributed to the PMMA in the MG49-NR.[12] These observations demonstrated the semicrystalline nature of MG49-NR. The XRD spectra of $Zn(CF_3SO_3)_2$ salt shows high intensity diffraction peaks at 2θ = 8.3°, 17.0°, 20.6°, 21.2°, 23.3°, 23.9°, 24.5°, 28.6°, 29.6°, 30.4°, 33.6°, 34.2°, 35.2°, 35.9°, 36.9°, 37.7°, and 39.9° confirm the high crystalline nature of the salt. Once the salt is blended with the MG49-NR polymer, the intense peaks observed in MG49-NR at 2θ = 29.5°, 36.0°, and 39.5° disappeared. This is due to the reduction of the semicrystalline nature in the polymer salt matrix. Moreover, all the observed diffraction peaks in the $Zn(CF_3SO_3)_2$ salt disappeared when it was blended with MG49-NR. This confirms that the $Zn(CF_3SO_3)_2$ salt is solvated well in the MG49-NR matrix. The diffraction peaks of the

Research Article
doi.org/10.1002/elsa.202300025
Chemistry Europe
European Chemical Societies Publishing

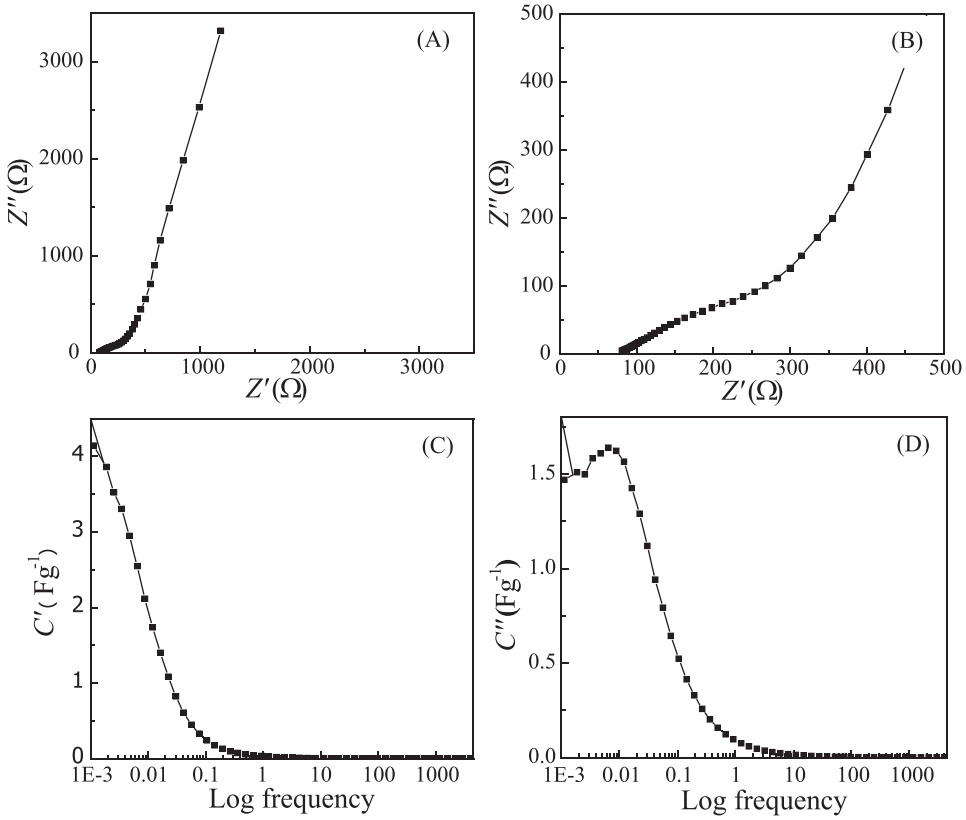

FIGURE 2 Nyquist plot of the supercapacitor obtained within the frequency range, (a) 4 kHz–0.001 Hz and (b) 4–500 kHz. (c) Variation of the real part of complex capacitance (C') with the frequency. (d) Variation of the imaginary part of complex capacitance (C'') with the frequency.

polymer-salt matrix at $2\theta = 7.6°$, 15.2°, 16.4°, 17.1°, 19.6°, 20.2°, 21.2°, 22.6°, 22.9°, 25.5°, 33.8°, 34.3°, 38.3°, and 38.6° confirm its crystallinity nature.

The supercapacitors were fabricated by sandwiching the MG49-NR + $Zn(CF_3SO_3)_2$ electrolyte between two identical graphite composite electrodes (see Supporting Information S1 for a detailed method). The fabricated supercapacitors were characterized by EIS, CV, and GCD. EIS is a powerful and widely used technique to analyze resistive and capacitive features of various materials and interfaces. It provides a deep insight into material and device characterization. Figure 2a,b shows the Nyquist plot drawn from the impedance data. In general, the low-frequency region of a Nyquist plot is very important for testing a supercapacitor because capacitive features become dominant at low frequencies. In a Nyquist plot, capacitive behavior is illustrated by a spike at a low-frequency region.[14] If pure capacitive features exist, a perfectly parallel line to the y-axis should be present. Figure 2b shows a spike at low frequency which confirms the capacitive features of the fabricated device. However, it is not perfectly parallel to the impedance (y) axis. The absence of a parallel line has been reported to be due to high resistance that may arise with difficulty in ion migration through the layered structure of graphite.[15] Theoretically, at the high-frequency region, a semicircle should be present showing bulk electrolyte features. The interception of the semicircle with the real axis of the Nyquist plot gives the bulk electrolyte resistance. Another semicircle appears at the mid-frequency region reflecting the charge transfer resistance at the electrolyte electrode interface. In the resulting Nyquist plot, the high-frequency semicircle is absent possibly due to the non-sufficient high-frequency region. However, bulk electrolyte resistance was found by the first intercept of the second semicircle. As per our results, the value of bulk electrolyte resistance is low (about 75 Ω) compared to NR (in the range of MΩ). This proves that MG49-NR-based electrolyte in the supercapacitor has a promising ionic conductivity which is an essential requirement for obtaining satisfactory performance. Charge transfer resistance is close to 150 Ω which is also small. This is also favorable for the satisfactory performance of a device.

Complex impedance data can be used to determine complex capacitance values, C' and C'' as shown in Equations (1) and (2).

$$C' = -Z'' / \omega\, |Z(\omega)| \quad (1)$$

Research Article
doi.org/10.1002/elsa.202300025
Chemistry Europe
European Chemical Societies Publishing

$$C'' = Z' / \omega \ |Z(\omega)| \quad (2)$$

where, Z' is the real part of complex impedance, Z'' is the imaginary part of complex impedance, $Z(\omega)$ is the complex impedance and ω is the angular frequency ($= 2\pi f$). C' and C'' were calculated using Equations (1) and (2), and the obtained impedance data.

The variation of C' with frequency is shown in Figure 2c. The value of C' is high at the low-frequency region, and it reduces to zero with increasing frequency. This clearly indicates that the capacitive and resistive features are dominating at low and high frequencies, respectively, and confirms the observation made with impedance data in the Nyquist plot.[16] The peak value of C' is related to the maximum single electrode specific capacitance (C_{sc}) of the supercapacitor, which is about 4.2 Fg^{-1} (31.9 $mFcm^{-2}$). In one of our previous studies, we fabricated and characterized a supercapacitor with the same electrolyte but with electrodes having only NG. It had nearly 1/3 lower C_{sc} value.[17] This difference is good evidence to propose the need for improving surface area when only NG is used for electrodes. However, the obtained value is small compared to reported values for supercapacitors with different configurations. Tey et al. reported a value of 112 $mFcm^{-2}$ for a supercapacitor fabricated with durian shell-based activated carbon electrodes and a liquid electrolyte.[18] Their larger value is possible due to the presence of a liquid electrolyte which shows higher performance than polymer electrolytes.

Figure 2d shows the variation of C'' with frequency, which is used to determine reaction rates within a particular device. In general, the rate of reactions that take place in a device plays a pivotal role in showcasing the performance of that device. The maximum C'' can be used to calculate the relaxation time constant, τ_0 which shows the rate of reactions leading to capacitive features. Hence, smaller τ_0 is always preferred as it relates to a faster reaction rate. Using Equation (3), the τ_0 was calculated from Figure 2d.[14]

$$\tau_0 = 1 / 2\pi f_0 \quad (3)$$

where f_0 is the frequency corresponding to the maximum C''. The calculated τ_0 is 26.5 s. Compared to reported values by several researchers for different supercapacitor configurations, this value is quite high.[18,19] This hints that the ion transfer process that is responsible for charge storage should be somewhat slower in the fabricated supercapacitor. It means that within the composite electrode or across the interface, ion movement may be hindered in spite of the fact that electrolyte has a substantial ionic conductivity.[17] Some possible reasons might be narrow ion conduction paths in the electrodes and a large gap between the electrode and the electrolyte.

The CV test can disclose many useful information such as the reduction and oxidation processes of molecular species and electron transfer-initiated chemical reactions.[20] While doing a CV test, the potential is varied within a pre-determined range and the change of current across a device/setup is measured and plotted as a current–potential graph which is called a cyclic voltammogram. Figure 3a shows the cyclic voltammogram of the supercapacitor obtained by varying the scan rate. In supercapacitors, if the electrodes are based on carbon materials such as graphite, graphene, etc., then the charge storage mechanism is based on the accumulation of opposite charges at and around the electrode-electrolyte interface, so-called "electrochemical double layer capacitors"—EDLCs. An important role is played by the scan rates in the process of charge storage. Hence, it is very vital to exploit how the scan rate affects the performance of supercapacitors.

In principle, no redox (faradaic) reactions which are known to arise due to oxidation and reduction reactions coupled with electrons take place in an EDLC. Such non-faradaic reactions are symbolized with cyclic voltammograms of rectangular shape. In Figure 3a, leafy shapes of cyclic voltammograms can be seen at high scan rates. However, the shape deviates to a rectangular shape while decreasing the scan rate, evidence of a non-faradaic reaction. This observation yields the fact that the ideal EDLC behavior of opposite charge accumulation at and around the electrode-electrolyte interface takes place at low scan rates. Similar behavior has been reported by Brza et al.[21] The leafy shape at a high scan rate may be due to poor charge accumulation around the interface. It is acceptable that at high scan rates, charges do not get sufficient time to undergo a complete reaction and as a result, proper accumulation cannot happen. As per the explanation made by Xie et al., the deviation of rectangular shapes at high scan rates may be due to dominant resistive features overriding capacitive features.[22] This fact is further supported and confirmed by the report of Liu et al.[23] They claimed that at high scan rates, there is a significant ohmic resistance exists for electrolyte ions to go into the electrodes. Also, all cyclic voltammograms show no peaks that are associated with redox reactions. The absence of peaks further proves that in the fabricated supercapacitor, charge storage takes place via non-faradaic reactions. Hadi et al., have observed and reported a similar result obtained for a supercapacitor developed with a biopolymer-based electrolyte and carbon-based electrodes.[24]

Research Article
doi.org/10.1002/elsa.202300025
Chemistry Europe
European Chemical Societies Publishing

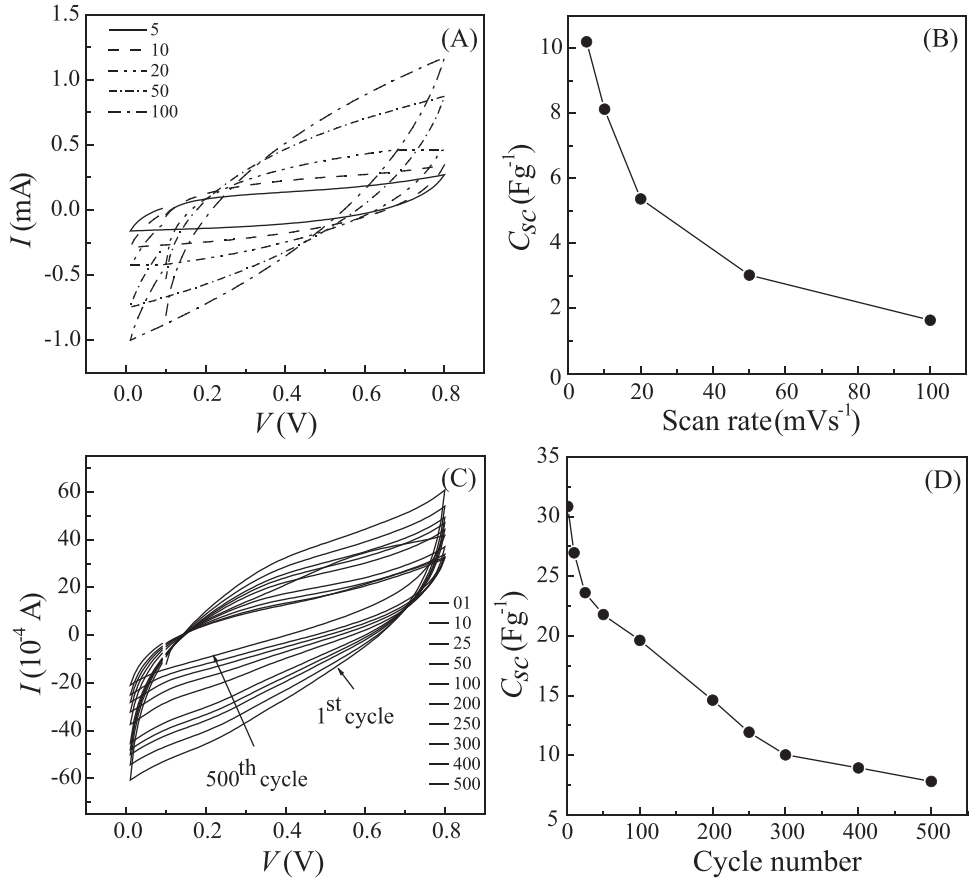

FIGURE 3 (a) Cyclic voltammograms at a constant current of 90 μA and different scan rates. (b) Variation of single electrode-specific capacitance (C_{sc}) with scan rate. (c) Cyclic voltammograms and (d) the variation of single electrode specific capacitance (C_{sc}) of 500 continuous cycles at a scan rate of 10 mVs^{-1}.

The single electrode specific capacitance, C_{sc} was calculated using Equation (4).

$$C_{sc} = 2 \int Idv/(mS\Delta V) \quad (4)$$

where $\int Idv$, m, S, and ΔV stand for the area under cyclic voltammogram, the mass of an electrode, scan rate, and potential window respectively. C_{sc} values were calculated for each scan rate and the variation of C_{sc} with scan rate is shown in Figure 3b. A notable feature in the figure is the decline of C_{sc} with increasing scan rate. This is a firm indication of the dependence of C_{sc} on the scan rate. At low scan rates, charges get ample time for diffusion into electrodes leading to high C_{sc}. But, when the charging-discharging process is taking place at high scan rates, charges cannot be involved with the complete storage process, and it leads to lower the C_{sc} values. This behaviour can also be associated with internal resistance that is assumed to be increasing with scan rate.[25,26]

Figure 3c shows several cyclic voltammograms obtained during the continuous cycling of the supercapacitor. The area of the curves reduces with time evidencing the declining performance of the supercapacitor. However, almost all cyclic voltammograms have a nearly rectangular shape evidencing the double-layer charge storage mechanism and non-faradic reactions. This confirms that the charge storage mechanism totally occurs via electrostatic reactions of charges throughout the continuous operation. The variation of C_{sc} with cycle number is shown in Figure 3d. The initial C_{sc} of 30.85 Fg^{-1} reduces to 7.82 Fg^{-1} during 500 cycles. The rate of deterioration is somewhat faster at the beginning but subsequently, it becomes slower. However, the retention of C_{sc} at 500th cycle is about 25% which is also a small value. But, in terms of the special features of the polymer electrolyte used for the present study such as safety and cost compared to commercial polymer-based solid electrolytes, obtained values are encouraging. Several research groups have reported the performance of supercapacitors with numerous carbon-based electrodes and biopolymers. Liew et al. obtained a C_{sc} value of 36.79 Fg^{-1} for the supercapacitor with two identical activated carbon, carbon black, poly(vinylidene fluoride) electrodes, and a biodegradable polymer + Li salt-based electrolyte.[27] When comparing the two salts, Li-based and Zn-based,

Research Article
doi.org/10.1002/elsa.202300025
Chemistry Europe
European Chemical Societies Publishing

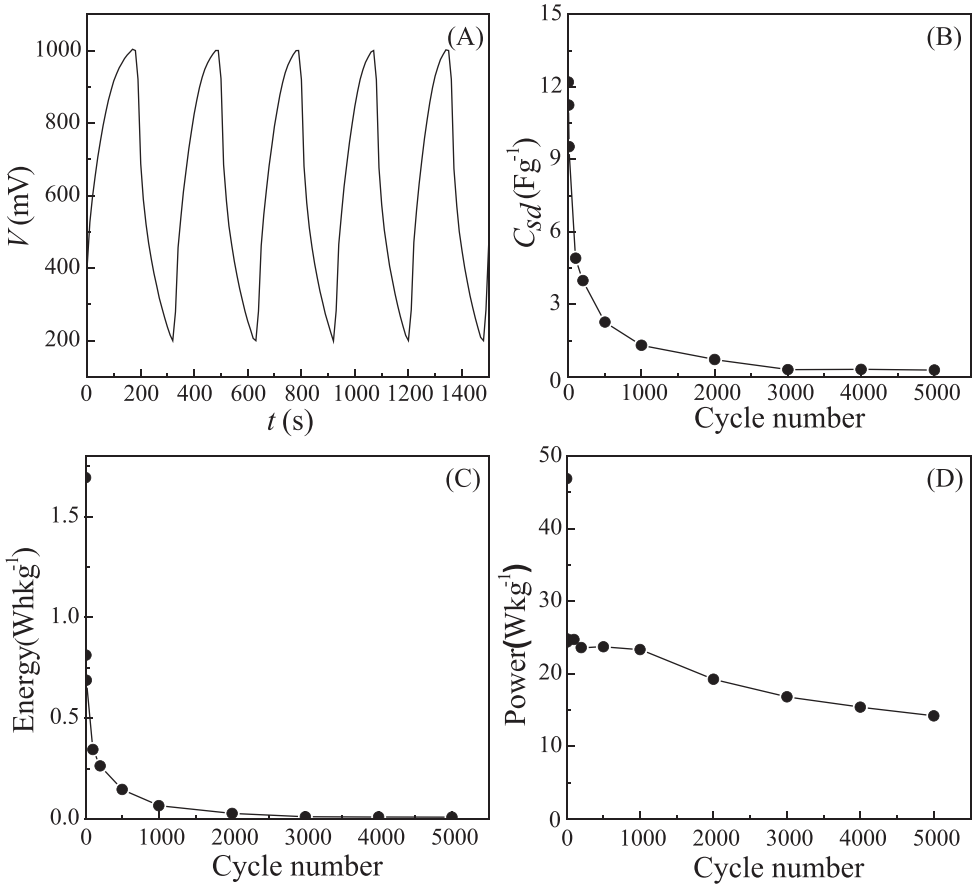

FIGURE 4 (a) Initial galvanostatic charge-discharge (GCD) curves during continuous cycling. (b) Variation of single electrode discharge capacitance, C_{sd}, (c) Variation of energy density, and (d) Variation of power density with cycle number.

high performance is usual in Li-based supercapacitors due to their monovalent cation.

The GCD study is shown in Figure 4. Figure 4a depicts a few initial cycles obtained from the continuous charge-discharge profiles of the supercapacitor. The presence of a linear discharge profile is an indication of the behavior of an EDLC. However, the non-perfectly linear GCD curves may be due to high resistance that may arise with difficulty in ion migration through the layered structure of graphite. The single electrode-specific discharge capacitance (C_{sd}) was calculated using Equation (5).

$$C_{sd} = Idt/mdV \tag{5}$$

where I is the constant current, dV/dt is the rate of potential drop excluding the drop due to internal resistance, and m is the mass of a single electrode. Potential drop due to internal resistance is seen with the transfer from charging mode to discharging mode as a sudden fall of potential. In the resultant profile of GCD curves, a notable fall could be observed indicating a high internal resistance. As per the explanation made by Hadi et al, this could be due to the resistive features of the current collector or an insufficient gap between the electrode and the electrolyte.[24]

The variation of specific discharge capacitance, C_{sd} during 5000 continuous cycles is shown in Figure 4b. The initial C_{sd} is about 12 Fg^{-1}. It dropped very fast till about the 100th cycle and reached around 0.2 Fg^{-1} at the 5000th cycle. The initial rapid decay of C_{sd} can be attributed to the absence of a well-formed interface soon after fabrication. During several charge-discharge cycles, the device is supposed to attain maturity and hence, interfaces become active. However, the reduction of C_{sd} over continuous cycling is suggestive of the formation of ion pairs and aggregates in the electrolyte, depletion of electrode-electrolyte interface as well as weakening of electrolyte. During charging and discharging, ions may be paired leading to ion pairs/aggregates that do not favor ion migration. This in turn lowers the number of ions accumulated at the electrode-electrolyte boundaries finally reducing C_{sd}. Teoh et al. have reported a closer C_{sd} value for a supercapacitor based on corn starch-based polymer electrolyte and activated carbon-based electrodes.[28] However, the reduction of C_{sd} over 500 cycles observed by them was very small.

Research Article
doi.org/10.1002/elsa.202300025

The dependence of energy density on number of cycles is shown in Figure 4c. The energy and power densities were calculated using Equations (6) and (7).

$$\text{Energy density, } E\ \left(\text{Whkg}^{-1}\right) = (1/2)\, C_{sd}\, V^2 \times 1000/3600 \tag{6}$$

$$\text{Power density, } P\ \left(\text{Wkg}^{-1}\right) = E \times 3600/t \tag{7}$$

where V is the voltage (V), and t is the discharge time (s). The first cycle shows an E of 1.69 Whkg^{-1} whereas it reduces to 0.02 Whkg^{-1} at the 5000th cycle. According to the Ragone plot, E values of supercapacitors should lie between 0.05 and 20 Whkg^{-1}.[29] The fabricated supercapacitor possesses that energy range of up to more than 1000 cycles. This is a promising result that expresses the suitability of this supercapacitor to be considered for further modifications. Figure 4d exhibits the variation of P under continuous cycling. Though the values are somewhat lower than reported values for some supercapacitors, they fall within the range stipulated by the Ragone plot.[29] The observed performance indicators of the present supercapacitors are lower compared to other different types of supercapacitors. However, as a novel study, the current investigation shows the suitability of the methyl-grafted NR-based electrolyte and the NG-based electrode to serve in supercapacitors. To get viable performance from the supercapacitor, there is paramount importance to improve the electrolyte and the electrode. From the side of the electrolyte, incorporating an ionic liquid as a substitute for the salt or adding redox additives as a mediator to induce pseudo-capacitive reactions at the interface would yield better results. Converting NG into graphene by any means would also be an effective approach to improve electrode performance. Upon satisfactory performance, the proposed supercapacitor would ideally address most of the demands expected from ideal energy storage devices in terms of performance, cost, and safety.

3 | CONCLUSION

A supercapacitor with MG49-NR + $Zn(CF_3SO_3)_2$ polymer-salt electrolyte and NG composite electrodes were successfully fabricated and characterized. ATR-FTIR and XRD measurements confirm that the $Zn(CF_3SO_3)_2$ salt solvated well into the MG49-NR polymer matrix. The impedance study of the fabricated supercapacitor confirms the dominant capacitive behavior at low frequencies and C_{sc} of 4.2 Fg^{-1}. From the CV test, it can be stated that charge storage takes place via non-Faradaic reactions and high C_{sc} is available with low scan rates. A quick drop of C_{sc} and C_{sd} was observed at the beginning of both CV and GCD tests. Even though the energy and the power densities are quite lower than reported literature values, this study proves the suitability of using methyl-grafted NR-based electrolytes and NG-based electrodes for supercapacitors. Since this is a sustainable device (low cost and user friendly in terms of non-toxic and easy to recycle), it is preferred to improve its performance via further modifications which include improving the structure of NG via ball milling and improving the electrolyte by substituting the salt with an ionic liquid or adding redox additives as a mediator to induce pseudo-capacitive reactions at the electrode-electrolyte interface.

4 | EXPERIMENTAL SECTION

All experiments and characterization techniques are provided in the Supporting Information.

ACKNOWLEDGMENTS

This work was supported by the Engineering and Physical Sciences Research Council (EPSRC) [under grant EP/Y003462/1], Keele University, and Wayamba University of Sri Lanka. The authors acknowledge Associated Speciality Rubbers (PVT) Ltd, Sri Lanka for providing the MG49-NR sample, Mr. K. Wickramaratne, Ragedara Mines (Pvt) Ltd, Sri Lanka for providing the NG sample, and Dr. Peter Matthews and Prof. Aleksandar Radu from Keele University for equipment support.

CONFLICT OF INTEREST STATEMENT

The authors declare no conflict of interest.

DATA AVAILABILITY STATEMENT

The data that support the findings of this study are openly available in the Keele Data Repository at https://doi.org/10.21252/7AXF-AS98.

ORCID

Nilanthy Balakrishnan https://orcid.org/0000-0002-7236-5477

REFERENCES

1. R. Wang, M. Yao, Z. Niu, *InfoMat* **2020**, *2*, 113.
2. P. K. Varshney, S. Gupta, *Ionics* **2011**, *17*, 479.
3. M. Rayung, M. M. Aung, S. C. Azhar, L. C. Abdullah, M. S. Su'ait, A. Ahmad, S. N. A. M. Jamil, *Materials* **2020**, *13*(4), 838.
4. A. Ahmad, M. Y. A. Rahman, M. S. Su'ait, H. Hamzah, *The Open Mater. Sci. J.* **2011**, *5*, 170
5. N. H. M. Zaki, Z. S. Mahmud, O. H. Hassan, M. Z. A. Yahya, A. M. M. Ali, *AIP Conf. Proc.* **2017**, *1875*, 020016.

6. C. Liu, Y. Liu, T. Yi, C. Hu, *Carbon* **2019**, *145*, 529.
7. Y. Lu, W. Jao, C. Tai, C. Hu, *J. Taiwan Inst. Chem. Eng.* **2023** (in press), https://doi.org/10.1016/j.jtice.2023.104978
8. R. Nandhini, P. A. Mini, B. Avinash, S. V. Nair, K. R. V. Subramanian, *Mater. Lett.* **2012**, *87*(15), 165.
9. Y. Wang, Z. J. Cao, Y. Zhou, J. Ouyang, D. Jia, L. Guo, *J. Electrochem. Soc.* **2012**, *159*(5) A579
10. M. Pandey, M. Balachandran, G. M. Joshi, N. N. Ghosh, A. S. Vendan, *J. Mater. Sci. Mater. Electron.* **2019**, *30*, 2136.
11. Y. Zhou, P. Jin, Y. Zhou, Y. Zhu, *Sci. Rep.* **2018**, *8*, 9005.
12. R. A. G. Whba, L. TianKhoon, M. S. Su'ait, M. Y. A. Rahman, A. Ahmad, *Arab. J. Chem.* **2020**, *13*, 3351.
13. C. M. Sai Prasanna, S. A. Suthanthiraraj, *Ionics* **2016**, *22*, 389.
14. N. O. Laschuk, E. B. Easton, O. V. Zenkina, *RSC Adv.* **2021**, *11*, 27925.
15. P. Sivaraman, A. P. Thakur, K. Shashidhara., *Synth. Met.* **2020**, *259*, 116255.
16. J. Wang, M. Chen, C. Wang, J. Wang, J. Zheng, *J. Power Sources* **2011**, *196*(1), 550.
17. N. Rajapaksha, K. S. Perera, K. P. Vidanapathirana, *Adv. Energy Res.* **2022**, *8*(1), 41.
18. J. P. Tey, M. A. Careem, M. A. Yarmo, A. K. Arof, *Ionics* **2016**, *22*, 1209.
19. R. Amade, A. Muyshegyan-Avetisyan, J. M. González, A. X. Martí Pino, E. György, E. Pascual, J. L. Andújar, E. B. Serra, *Materials* **2019**, *12*, 483.
20. N. Elgrishi, K. J. Rountree, B. D. McCarthy, E. S. Rountree, T. T. Eisenhart, J. L. Dempsey, *J. Chem. Educ.* **2018**, *95*(2), 197.
21. M. A. Brza, S. B. Aziz, H. Anuar, E. M. A. Dannoun, F. Ali, R. T. Abdulwahid, S. Al-Zangana, M. F. Z. Kadir, *Polymers* **2020**, *12*(9), 1896.
22. Y. Xie, H. Du, *RSC Adv.* **2015**, *5*, 89689.
23. H. Liu, K. Wang, H. Teng, *Carbon* **2005**, *43*, 559.
24. J. M. Hadi, S. B. Aziz, M. A. Brza, M. F. Z. Kadir, R. T. Abdulwahid, B. A. Al-Asbahi, A. A. Ali Ahmed, *Alexandria Eng. J.l* **2022**, *61*(12), 9273.
25. E. M. A. Dannoun, S. B. Aziz, M. A. Brza, M. M. Nofal, A. S. F. M. Asnawi, Y. M. Yusof, S. Al-Zangana, M. H. Hamsan, M. F. Z. Kadir, H. J. Woo, *Polymers* **2020**, *12*, 2531.
26. X. You, M. Misra, S. Gregori, A. K. Mohanty, *ACS Sustainable Chem. Eng.* **2018**, *6*(1), 318.
27. C. Liew, S. Ramesh, *Carbohydr. Polym.* **2015**, *124*, 222.
28. K. H. Teoh, C. Lim, C. W. Liew, S. Ramesh, *J. Appl. Polym. Sci.* **2016**, 43275.
29. S. K. Poonam, A. Arora, S. K. Tripathi, *J. Energy Storage* **2019**, *21*, 801.

SUPPORTING INFORMATION

Additional supporting information can be found online in the Supporting Information section at the end of this article.

How to cite this article: K. S. Perera, K. P. Vidanapathirana, L. J. Adams, N. Balakrishnan, *Electrochem. Sci. Adv.* **2023**, e2300025. https://doi.org/10.1002/elsa.202300025